# Data-driven Stochastic Robust Energy Management for Multi-stage Cascade Utilization of Liquefied Natural Gas Cold Energy in Multi-energy Microgrid

Bo Wang, *Member*, *IEEE*, Zhehan Jia, Xingying Chen, *Senior Member*, *IEEE*, Lei Gan, *Member*, *IEEE*, Haochen Hua, *Member*, *IEEE*, Kun Yu, *Senior Member*, *IEEE*, and Jun Shen

***Abstract*—Liquefied natural gas (LNG), recognized as the primary form for natural gas transportation, can release substantial cold energy during gasification. To make efficient use of this cold energy, this paper proposes a data-driven stochastic robust (DDSR) energy management method for the multi-stage cascade utilization of LNG cold energy in a multi-energy microgrid (MEMG) of an LNG receiving terminal. Firstly, a general scheduling model considering the flexible coupling between adjacent stages, energy losses, and electric power consumption for the cascade utilization of LNG cold energy is introduced. This model is applied to carbon capture, cryogenic power generation, and direct cooling, which are sequentially associated with the deep, medium, and shallow cooling zones of LNG cold energy, respectively. Moreover, a two-stage energy management framework is proposed to coordinate the cascade utilization of LNG cold energy with other energy resources in the MEMG. To tackle the uncertainties of renewable energy generation and various loads, a DDSR-based solution method is developed, aiming to achieve both economic benefits and solution robustness by identifying the worst-case scenarios and the corresponding worst-case probability. Accordingly, a Benders decomposition-based solution algorithm is proposed to divide the original problem into a master problem and a slave problem, which are solved iteratively. The simulation results verify the effectiveness and high efficiency of the proposed DDSR energy management method for multi-stage cascade utilization of LNG cold energy.**

***Index Terms*—Energy management, stochastic robust optimization, liquefied natural gas (LNG), cold energy, multi-energy microgrid.**

## I. Introduction

NATURAL gas (NG) is widely recognized as a clean fossil fuel, and its demand has been experiencing substantial growth in the context of carbon neutrality and energy transition [1]. Upstream NG is transported in the form of liquefied natural gas (LNG) by ocean-going vessels to LNG receiving terminals. Upon arrival at these terminals, LNG is gasified before being delivered to end-users [2]. During the gasification process, approximately 830 kJ of cold energy is released per kilogram of LNG [3]. Given that the global annual consumption of LNG can reach as high as 39.64 billion tons annually [4], harnessing the released cold energy during LNG gasification can bring significant opportunities for a wide range of energy applications. However, many LNG receiving terminals use seawater as a natural heat source for vaporizing and warming LNG, leading to a significant waste of cold energy. Thus, it is important to explore the effective utilization of LNG cold energy and to realize great social, economic, and environmental benefits [5].

The existing technologies of LNG cold energy utilization can be categorized according to different temperature zones of cold energy. The low-temperature carbon capture [6], light hydrocarbon separation [7], and seawater desalination [8] mainly utilize cold energy from the deep cooling zone. In contrast, cryogenic power generation [9] primarily utilizes LNG cold energy from the medium cooling zone. Additionally, the shallow cooling zone of LNG cold energy can be used for air-conditioning refrigeration [10] and cold storage [11]. Therefore, integrating these various applications into a comprehensive energy system that utilizes LNG cold energy stepwise through multiple temperature zones can significantly enhance energy utilization efficiency and bring substantial economic and environmental advantages [12].

Extensive research efforts have been devoted to the utilization of LNG cold energy. Reference [13] introduces an integrated power and cooling system that incorporates a cascade organic Rankine cycle (ORC) system, an air-conditioning refrigeration, and a direct expansion cycle. Thermodynamic and economic evaluation are performed along with parameter optimization, aiming to maximize the utilization of LNG

Manuscript received: May 22, 2025; revised: August 4, 2025; accepted: September 1, 2025. Date of CrossCheck: September 1, 2025. Date of online publication: September 29, 2025.

This work was supported in part by the National Natural Science Foundation of China (No. 52307091), in part by the Natural Science Foundation of Jiangsu Province (No. BK20230952), and in part by the China Postdoctoral Science Foundation (No. 2023M740976).



B. Wang, Z. Jia, X. Chen (corresponding author), L. Gan, H. Hua, and K. Yu are with the School of Electrical and Power Engineering, Hohai University, Nanjing 211100, China (e-mail: bowangee@hhu.edu.cn; zhjia2025@163.com; xychen@hhu.edu.cn; leigan@hhu.edu.cn; huahc16@tsinghua.org.cn; kunyu@hhu.edu.cn).

J. Shen is with the School of Mechanical Engineering, Beijing Institute of Technology, Beijing 100081, China (e-mail: jshen@bit.edu.cn).

DOI: 10.35833/MPCE.2025.000456

cold energy. Reference [6] employs a concept of cascade-nested ORC cycles to develop a combined system for power generation and $CO_2$ capture based on LNG cold energy in the magnesite processing industry. The system performance is improved by selecting optimal mixed working fluids and incorporating regenerators. Furthermore, an LNG cold energy cascade utilization system that integrates light hydrocarbon separation, ORC-based power generation with data center cooling, as well as warehouse cold storage, is proposed in [10]. Moreover, [14] develops a cascade integrated system for electricity, cooling, heating, and freshwater production using a gas turbine and desalination in conjunction with LNG gasification. Thermodynamic, environmental, and economic analyses indicate a notable improvement in the operation efficiency and environmental sustainability. Reference [15] designs a combined LNG gasification and liquid air energy storage system, which applies parallel two-stage Rankine cycles for power generation during peak periods and energy storage during off-peak periods, thereby enhancing the system flexibility, safety, and operational profitability. Overall, the above studies illustrate the significance of cascade utilization of LNG cold energy in energy efficiency and economic benefits, but they primarily focus on the design and thermodynamic simulation of the LNG cold energy utilization system.

With the advancement of the green and low-carbon transition [16], the LNG receiving terminal can be equipped with abundant renewable and flexible energy resources to meet diverse energy demands, forming a multi-energy microgrid (MEMG) [17]. At present, there are few studies on the scheduling level of LNG cold energy utilization in coordination with other energy resources. Reference [18] proposes a day-ahead (DA) dispatch model that coordinates the liquid air storage and LNG gasification. The cold energy from LNG gasification is only used for air liquefaction, which may lead to a low utilization efficiency of LNG cold energy. Moreover, an MEMG scheduling model considering a three-stage cascade utilization of cold energy for carbon capture, power generation, and direct cooling is proposed in [19]. This model pre-assigns a fixed range of cold energy to the three applications without capturing the flexible interactions between adjacent stages, and also ignores the energy loss and electric power consumption during the cascade utilization process of cold energy.

In addition, to address the uncertainties of renewable energy generation and loads, stochastic optimization (SO) and robust optimization (RO) methods are often applied. The SO method [20] determines the optimal expected objective with multiple sampled uncertainty scenarios based on the probability distribution of uncertainties. However, the probability distribution may be unknown or inaccurate. Alternatively, the RO method [21] optimizes decisions under the worst-case uncertainties characterized by a low probability of occurrence, resulting in a conservative result. Therefore, it is important to develop an optimization method that can address the disadvantages of SO and RO methods. With the digitalization of MEMG, more available historical data of uncertainties can be collected to support the MEMG operation. Conventional data-driven distributionally robust optimization method [22] utilizes finite uncertainty scenarios (historical data) with similar features to make decisions under the worst probability distribution belonging to an ambiguity set using $1/\infty$ norms [23] or Wasserstein ball [24], [25] measurements. However, these uncertainty samples may not always reoccur.

Meanwhile, it is rational to assume that the realization of uncertainties tends to be concentrated around each similar historical and prediction scenario within a small variation interval [26], which can trace the trajectory of uncertainty profiles. By searching for the worst case in each interval and the corresponding worst-case probability distribution with overall variation control, a certain level of solution robustness can be preserved while maintaining the economic benefits. Thus, based on this principle, this paper develops a data-driven solution method to address the uncertainties in MEMG energy management.

In summary, although existing research offers valuable insights into the cascade utilization of LNG cold energy, there remain limitations in scheduling-level modelling of cascade utilization of LNG cold energy and the associated energy management under uncertainties. To address these challenges, this paper proposes a data-driven stochastic robust (DDSR) energy management method for multi-stage cascade utilization of LNG cold energy in an MEMG. The main contributions are summarized as follows.

1) A general scheduling model for the cascade utilization of LNG cold energy is introduced and applied to carbon capture, cryogenic power generation, and direct cooling. This model considers the flexible coupling between adjacent utilization stages, energy losses, and electric power consumption.

2) By taking into account the operating characteristics of the MEMG, a two-stage energy management framework is proposed to coordinate the cascade utilization of LNG cold energy with other energy resources in the MEMG.

3) To address the uncertainties of renewable energy generation and various loads, a DDSR-based solution method is developed, aiming to achieve both economic benefits and solution robustness by identifying the worst-case scenarios and the corresponding worst-case probability.

The remainder of this paper is organized as follows. Section II introduces the two-stage energy management framework. Section III presents a general scheduling model for the cascade utilization of LNG cold energy, and Section IV provides the mathematical formulation of MEMG energy management. A DDSR-based solution method is proposed in Section V. Then, Section VI presents case study to verify the effectiveness and high efficiency of the proposed DDSR energy management method. Lastly, Section VII concludes this paper and provides the direction of future work.

## II. Two-stage Energy Management Framework

This section introduces the two-stage energy management framework for the cascade utilization of LNG cold energy. The MEMG structure and energy flows are shown in Fig. 1, where $P_t^{Buy}$ and $P_t^{Sell}$ are the power purchased from and sold to the power grid, respectively. Other variables will be explained in the following text.

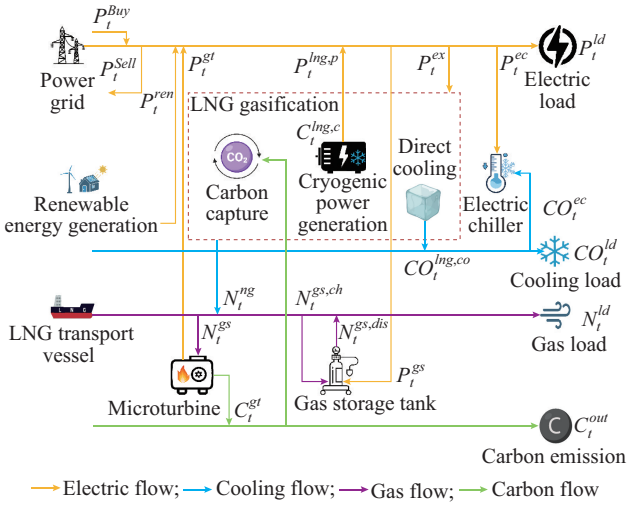


Fig. 1. MEMG structure and energy flows.

The LNG receiving terminal-based MEMG needs to fulfill various energy demands including electric, cooling, and gas loads with the goal of minimizing operation costs and carbon emissions. To make efficient use of LNG cold energy, the cascade utilization in the LNG gasification station comprises carbon capture, cryogenic power generation, and direct cooling that are sequentially associated with the deep, medium, and shallow cooling zones of LNG cold energy, respectively. Moreover, the MEMG is mainly equipped with renewable energy generation, microturbine, electric chiller, gas storage tank, together with these three applications of LNG cold energy, to meet various electricity, cooling, and gas demands. Accordingly, there are four distinct energy flows including electric flow, cooling flow, gas flow, and carbon flow, which are mutually coupled. The carbon emission from the microturbine generation is mitigated by the carbon capture process. Electric chiller combines with the direct cooling process to satisfy the cooling requirement. Considering that the total released cold energy depends on the gas demand, gas storage tank serves as a buffer between the gasified LNG and the actual gas load to improve the utilization flexibility of LNG cold energy. Lastly, the MEMG can purchase or sell energy in the DA electricity market and intraday hourly-ahead (HA) electricity market.

Considering the operating characteristics of the MEMG, a two-stage energy management framework is established. In the DA stage, the on/off states of LNG gasification, the multi-stage utilization processes of cold energy, and microturbines are determined based on the whole-day predictions of uncertain renewable energy generation and various loads. Also, the energy transaction in the DA market is optimized. Subsequently, in the HA stage of the next day, the output production of LNG equipment, the power outputs of flexible resources, and the HA energy transaction are optimized using more accurate short-term predictions of uncertainties to meet various load demands with an economic and low-carbon objective for MEMG operation.

## III. General Scheduling Model for Cascade Utilization of LNG Cold Energy

This section introduces a general scheduling model for the cascade utilization of LNG cold energy. For ease of description, each stage of cold energy utilization is indexed by $m$.

### A. LNG Gasification

The constraints for LNG gasification are given as:

$$\alpha_t^{ng} N_{\min}^{ng} \le N_t^{ng} \le \alpha_t^{ng} N_{\max}^{ng} \quad \forall t \tag{1}$$

$$CE_t^{lng} = N_t^{ng} \rho_{ng} \eta_{ce} \left( h + c_{ng} \Delta T \right) c_{kwh} \quad \forall t \tag{2}$$

where subscript $t$ is the index of scheduling time interval; $\alpha_t^{ng}$ is the binary on/off state of the gasification process; $N_t^{ng}$ is the gasified NG volume; $N_{\min}^{ng}$ and $N_{\max}^{ng}$ are the minimum and maximum gasified NG volumes, respectively; $CE_t^{lng}$ is the total released cold energy; $\rho_{ng}$ is the NG density; $\eta_{ce}$ is the recovery efficiency of LNG cold energy; $c_{ng}$ is the average specific heat capacity of NG; $\Delta T$ is the temperature change during the gasification process; $h$ is the latent heat of phase transition from LNG to NG; and $c_{kwh}$ is a coefficient that converts unit kJ to kWh, which is normally 1/3600.

Constraint (1) limits the LNG gasification within the rated range. The total released cold energy is calculated by (2), which comprises the latent heat caused by phase change from liquid to gas and the sensible heat associated with the temperature change of NG. It is noted that the difference between the storage temperature and the boiling point of LNG is small. Therefore, the related cold energy resulting from the temperature change in the LNG form is neglected in this paper.

Furthermore, the LNG gasification equipment may not start or stop arbitrarily, and thus should comply with specific on/off time limits, which are constrained as:

$$\alpha_\varepsilon^{ng} \ge \alpha_t^{ng} - \alpha_{t-1}^{ng} \quad \forall \varepsilon \in \left[ t+1, t+T_{on}^{ng} - 1 \right] \tag{3}$$

$$\alpha_\varepsilon^{ng} \le 1 - \left( \alpha_{t-1}^{ng} - \alpha_t^{ng} \right) \quad \forall \varepsilon \in \left[ t+1, t+T_{off}^{ng} - 1 \right] \tag{4}$$

where $T_{on}^{ng}$ and $T_{off}^{ng}$ are the minimum on-time and off-time limits, respectively; and $\varepsilon$ is the selected scheduling time interval within the given periods.

### B. General Single-stage Utilization of LNG Cold Energy

Considering the application of each utilization stage, there are the minimum and maximum amounts of input cold energy for the normal operation. The utilized cold energy for each stage is constrained as:

$$\alpha_t^m \cdot CE_{\min}^m \le CE_t^m \le \alpha_t^m \cdot CE_{\max}^m \quad \forall t \tag{5}$$

where $CE_{\min}^m$ and $CE_{\max}^m$ are the minimum and maximum limits of the input cold energy in stage $m$, respectively; $\alpha_t^m$ is the binary on/off state of the utilization process of cold energy; and $CE_t^m$ is the input cold energy in stage $m$.

The cold energy utilization equipment also needs to adhere to specific on-time and off-time limits. $T_{on}^m$ and $T_{off}^m$ represent the minimum on-time and off-time limits for the cold energy utilization equipment in stage $m$, respectively. These constraints can be referred to (3) and (4).

During the utilization process of cold energy, the cold energy losses occur due to heat exchange, heat transfer, and energy conversion. Also, some components such as pumps, compressors, and expanders consume electricity. Therefore, it is important to consider both energy losses and electric power consumption during the utilization of cold energy, as specified in (6) and (7), respectively.

$$CELS_t^m = f_l\left(CE_t^m\right) \quad \forall t, \forall m \tag{6}$$

$$PC_t^m = f_p\left(CE_t^m - CELS_t^m\right) \quad \forall t, \forall m \tag{7}$$

where $CELS_t^m$ is the cold energy loss in stage $m$; $PC_t^m$ is the electric power consumption during the utilization process of cold energy in stage $m$; $f_l(\cdot)$ is the relationship function between the cold energy losses and the input cold energy; and $f_p(\cdot)$ is the relationship function between the electric power consumption and the utilized cold energy.

Lastly, the utilized cold energy is converted into the target product in each stage. The output production of the LNG cold energy utilization is expressed as:

$$M_t^{lng,m} = f_o\left(CE_t^m - CELS_t^m\right) \quad \forall t, \forall m \tag{8}$$

where $M_t^{lng,m}$ is the output production of the cold energy utilization in stage $m$; and $f_o(\cdot)$ is the relationship function between the output and the utilized cold energy.

This paper assumes that $f_l(\cdot)$, $f_p(\cdot)$, and $f_o(\cdot)$ are linear functions. Thus, (6)-(8) can be rewritten as:

$$CELS_t^m = \mu_m \cdot CE_t^m \quad \forall t, \forall m \tag{9}$$

$$PC_t^m = k_m\left(CE_t^m - CELS_t^m\right) \quad \forall t, \forall m \tag{10}$$

$$M_t^{lng,m} = \eta_m\left(CE_t^m - CELS_t^m\right) \quad \forall t, \forall m \tag{11}$$

where $\mu_m$ is the loss coefficient; $k_m$ is the coefficient of electric power consumption; and $\eta_m$ is the utilization rate of LNG cold energy. It is noted that adopting other functions does not affect the effectiveness of the proposed general model for LNG cold energy utilization.

### C. Cascade Utilization of LNG Cold Energy

With the above single-stage utilization, the cascade utilization of LNG cold energy can be modelled as:

$$CE_t^{lng} \geq \sum_m CE_t^m \quad \forall t \tag{12}$$

$$P_t^{ex} = \sum_m PC_t^m \quad \forall t \tag{13}$$

where $P_t^{ex}$ is the total electric power consumption through all stages.

Constraint (12) indicates that the aggregated input cold energy of all the stages cannot exceed the total released cold energy from LNG gasification. With constraints (5) and (12), it is evident that if one utilization stage consumes less cold energy, more available cold energy will remain in other stages, showing a flexible coupling between adjacent stages. Then, the total electric power consumption of the cascade utilization of LNG cold energy is expressed by (13).

## IV. Mathematical Formulation of MEMG Energy Management

The MEMG has abundant renewable and flexible energy resources which can be coordinated with the cascade utilization of LNG cold energy to achieve highly efficient energy management. In this section, the mathematical formula of MEMG energy management is developed for the multi-stage cascade utilization of LNG cold energy.

In the following text, the aforementioned utilization stage $m$ is replaced by $c$, $p$, and $co$, which correspond to the carbon capture stage, the cryogenic power generation stage, and the direct cooling stage, respectively. Moreover, the output production $M$ is replaced by $C$, $P$, and $CO$, representing the captured carbon quantity, generated power, and produced cooling power, respectively.

### A. Constraints of Renewable and Flexible Energy Recources

*1) Renewable Energy Generation*

$$0 \leq P_t^{ren} \leq P_{\max}^{ren} \quad \forall t \tag{14}$$

where $P_t^{ren}$ is the renewable energy generation power; and $P_{\max}^{ren}$ is its maximum value.

*2) Gas Storage Tank*

$$S_t^{gs} = S_{t-1}^{gs} + \left(N_t^{gs,ch} - N_t^{gs,dis}\right)\frac{\tau}{\eta_{gs} V_{gs}} \quad \forall t \tag{15}$$

$$S_{\min}^{gs} \leq S_t^{gs} \leq S_{\max}^{gs} \quad \forall t \tag{16}$$

$$0 \leq N_t^{gs,ch} \leq \alpha_t^{gs} N_{\max}^{gs} \quad \forall t \tag{17}$$

$$0 \leq N_t^{gs,dis} \leq \left(1 - \alpha_t^{gs}\right) N_{\max}^{gs} \quad \forall t \tag{18}$$

$$S_0^{gs} = S_{24}^{gs} \tag{19}$$

$$P_t^{gs} = k_{gs}\left(N_t^{gs,ch} + N_t^{gs,dis}\right) \quad \forall t \tag{20}$$

where $S_t^{gs}$ is the state of charge (SoC) of the gas storage tank; $\tau$ is the scheduling time interval; $V_{gs}$ is the nominal capacity of the gas storage tank; $\eta_{gs}$ is the compression rate; $S_{\min}^{gs}$ and $S_{\max}^{gs}$ are the minimum and maximum SoC limits of the gas storage tank, respectively; $S_0^{gs}$ and $S_{24}^{gs}$ are the initial SoC and last SoC, respectively; $\alpha_t^{gs}$ is the binary charging/discharging state; $N_t^{gs,ch}$ and $N_t^{gs,dis}$ are the charging and discharging flow rates of NG, respectively; $N_{\max}^{gs}$ is the maximum charging/discharging flow rate; $k_{gs}$ is the electric power consumption coefficient; and $P_t^{gs}$ is the electric power consumption of the gas storage tank.

The SoC of the gas storage tank is calculated by (15) and constrained by (16). Constraints (17) and (18) limit the charging and discharging flow rates of NG for the gas storage tank, respectively. Constraint (19) ensures that the last SoC is equal to the initial SoC. Constraint (20) calculates the electric power consumption of the gas storage tank. It is noted that other types of energy storage can be considered to further enhance the temporal coordination capability and flexibility of the MEMG.

*3) Microturbine*

$$P_t^{gt} = \eta_{gt} N_t^{gt} \quad \forall t \tag{21}$$

$$\alpha_t^{gt} P_{\min}^{gt} \leq P_t^{gt} \leq \alpha_t^{gt} P_{\max}^{gt} \quad \forall t \tag{22}$$

$$P_{t-1}^{gt}-P_t^{gt}\le r_{\max}^{gt}\quad \forall t \tag{23}$$

$$P_t^{gt}-P_{t-1}^{gt}\le r_{\max}^{gt}\quad \forall t \tag{24}$$

$$C_t^{gt}=\lambda_{g,co2}N_t^{gt}\quad \forall t \tag{25}$$

where $P_t^{gt}$ is the electric power of the microturbine; $N_t^{gt}$ is the consumed NG for electric power generation; $\eta_{gt}$ is the conversion efficiency; $\alpha_t^{gt}$ is the binary on/off state of the microturbine; $P_{\min}^{gt}$ and $P_{\max}^{gt}$ are the minimum and maximum power limits of the microturbine, respectively; $r_{\max}^{gt}$ is the maximum ramping rate; $C_t^{gt}$ is the carbon emission of the microturbine; and $\lambda_{g,co2}$ is the carbon emission coefficient.

The electric power generation of the microturbine with respect to the NG consumption is described by (21). Constraint (22) limits the power generation. Constraints (23) and (24) restrict the ramping rate. The carbon emission of the microturbine is calculated by (25). Additionally, if the minimum on-/off-time limits are necessary, these limits can be referred to (3) and (4).

*4) Electric Chiller*

$$CO_t^{ec}=\eta_{ec}P_t^{ec}\quad \forall t \tag{26}$$

$$0\le CO_t^{ec}\le CO_{\max}^{ec}\quad \forall t \tag{27}$$

where $CO_t^{ec}$ is the produced cooling power of the electric chiller; $P_t^{ec}$ is the electric power consumption of the electric chiller; $\eta_{ec}$ is the refrigeration efficiency; and $CO_{\max}^{ec}$ is the maximum cooling power.

Equation (26) describes the produced cooling power with respect to the electric power consumption, and (27) constrains the cooling power.

### *B. Mathematical Formula of MEMG Energy Management*

Aiming at a low-carbon and economic operation, a MEMG energy management model considering the cascade utilization of LNG cold energy is proposed as:

$$\min \sum_t \left(C_t^{tra}+C_t^{co2}+C_t^{lng}+C_t^{su}\right) \tag{28}$$

s.t.

(1)-(5), (9)-(27)

$$C_t^{tra}=C_t^{tra,da}+C_t^{tra,ha}\quad \forall t \tag{29}$$

$$C_t^{tra,da}=\left(pr_t^{Bda}P_t^{Bda}-pr_t^{Sda}P_t^{Sda}\right)\tau\quad \forall t \tag{30}$$

$$C_t^{tra,ha}=\left(pr_t^{Bha}P_t^{Bha}-pr_t^{Sha}P_t^{Sha}\right)\tau\quad \forall t \tag{31}$$

$$C_t^{co2}=c_{co2}C_t^{out}\quad \forall t \tag{32}$$

$$C_t^{lng}=c_c^{lng}C_t^{lng,c}+c_p^{lng}P_t^{lng,p}+c_{co}^{lng}CO_t^{lng,co}\quad \forall t \tag{33}$$

$$C_t^{su}=c_{su}^{ng}u_t^{ng}+c_{su}^{gt}u_t^{gt}+\sum_m c_{su}^m u_t^m\quad \forall t \tag{34}$$

$$u_t^{\gamma}\ge \alpha_t^{\gamma}-\alpha_{t-1}^{\gamma}\quad \forall t,\gamma=ng,gt,m \tag{35}$$

$$P_t^{Bda}+P_t^{Bha}+P_t^{gt}+P_t^{ren}+P_t^{lng,p}=P_t^{Sda}+P_t^{Sha}+P_t^{ld}+P_t^{ex}+P_t^{ec}+P_t^{gs}\quad \forall t \tag{36}$$

$$N_t^{ng}+N_t^{gs,dis}=N_t^{gt}+N_t^{ld}+N_t^{gs,ch}\quad \forall t \tag{37}$$

$$CO_t^{ec}+CO_t^{lng,co}=CO_t^{ld}\quad \forall t \tag{38}$$

$$C_t^{gt}=C_t^{out}+C_t^{lng,c}\quad \forall t \tag{39}$$

$$0\le \sum_t C_t^{out}\le C_{\max}^{out} \tag{40}$$

$$\begin{cases}0\le P_t^{Bda}\le P_{\max}^{line}\\ 0\le P_t^{Sda}\le P_{\max}^{line}\end{cases}\quad \forall t \tag{41}$$

$$\begin{cases}0\le P_t^{Bha}\le P_{\max}^{line}\\ 0\le P_t^{Sha}\le P_{\max}^{line}\end{cases}\quad \forall t \tag{42}$$

$$0\le P_t^{Bda}-P_t^{Sda}+P_t^{Bha}-P_t^{Sha}\le P_{\max}^{line}\quad \forall t \tag{43}$$

where $C_t^{tra}$ is the total transaction cost; $C_t^{co2}$ is the carbon emission cost; $C_t^{lng}$ is the operation cost of LNG cold energy utilization, $C_t^{su}$ is the startup cost; $C_t^{tra,da}$ and $C_t^{tra,ha}$ are the DA and intraday HA transaction costs, respectively; $pr_t^{Bda}$ and $pr_t^{Bha}$ are the DA and intraday HA purchasing prices, respectively; $pr_t^{Sda}$ and $pr_t^{Sha}$ are the DA and intraday HA selling prices, respectively; $P_t^{Bda}$ and $P_t^{Bha}$ are the DA and intraday HA purchasing power, respectively; $P_t^{Sda}$ and $P_t^{Sha}$ are the DA and intraday HA selling power, respectively; $c_{co2}$ is the carbon tax price; $C_t^{out}$ is the carbon emission; $C_{\max}^{out}$ is the daily carbon emission limit; $c_c^{lng}$, $c_p^{lng}$, and $c_{co}^{lng}$ are the unit operation costs for carbon capture, cryogenic power generation, and direct cooling, respectively; $C_t^{lng,c}$, $P_t^{lng,p}$, and $CO_t^{lng,co}$ are the reduced carbon emissions from carbon capture, the output power of cryogenic power generation, and the direct cooling power, respectively; $c_{su}^{ng}$, $c_{su}^{gt}$, and $c_{su}^{m}$ are the start-up costs of the LNG gasification, microturbine, and cold energy utilization equipment in stage $m$, respectively; $u_t^{\gamma}$ is a binary startup indicator of the related equipment $\gamma$; $P_t^{ld}$, $N_t^{ld}$, and $CO_t^{ld}$ are the electric, gas, and cooling loads, respectively; and $P_{\max}^{line}$ is the maximum line capacity for the DA or intraday HA electricity transactions.

The objective function (28) minimizes the total operation costs of the MEMG system, including the transaction cost, carbon emission cost, operation cost of LNG equipment, and the start-up cost, which are described in (29)-(34), respectively. Constraint (35) defines the startup indicator of the related equipment. Moreover, energy balances of the electric flow, gas flow, cooling flow, and carbon flow are specified in (36)-(39). The daily carbon emission is limited by (40). Constraints for purchasing and selling electricity in DA and intraday HA markets are given in (41) and (42), respectively. And finally, the total power exchange with the upstream grid is limited by (43). It is worth noting that minimizing the transaction cost implies reducing the electric energy exchange with the upstream grid. Given that the purchasing prices are typically higher than the selling prices, the MEMG system prioritizes maximizing the consumption of its internal energy, thereby enhancing the overall efficiency of energy utilization.

## V. DDSR-based Solution Method

The uncertainties of renewable energy outputs and various loads can impair the MEMG operation. To deal with them, a DDSR-based solution method is developed in this section.

Firstly, historical data with the features similar to the next day and prediction data are aggregated to produce uncertainty scenarios. With these uncertainty scenarios, the proposed energy management model of the LNG receiving terminal-

based MEMG in Section IV can be reformulated to the following stochastic compact form as:

$$\min_{\boldsymbol{x}} \boldsymbol{A}^{\mathrm{T}}\boldsymbol{x} + \min_{\boldsymbol{y}_s} \sum_{s=1}^{N_s} \rho_s \boldsymbol{B}^{\mathrm{T}}\boldsymbol{y}_s \tag{44}$$

s.t.

$$\boldsymbol{C}\boldsymbol{x} \le \boldsymbol{d} \tag{45}$$

$$\boldsymbol{E}\boldsymbol{x} + \boldsymbol{F}\boldsymbol{y}_s + \boldsymbol{G}\boldsymbol{u}_s = \boldsymbol{w} \quad \forall s \tag{46}$$

$$\boldsymbol{H}\boldsymbol{x} + \boldsymbol{I}\boldsymbol{y}_s \le \boldsymbol{v} \quad \forall s \tag{47}$$

where $\boldsymbol{A}$, $\boldsymbol{B}$, $\boldsymbol{C}$, $\boldsymbol{E}$, $\boldsymbol{F}$, $\boldsymbol{G}$, $\boldsymbol{H}$, and $\boldsymbol{I}$ are the coefficient matrices; $\boldsymbol{d}$, $\boldsymbol{w}$, and $\boldsymbol{v}$ are the coefficient vectors; subscript $s$ denotes the index of uncertainty scenarios with the total number $N_s$; $\rho_s$ is the probability of occurrence for each uncertainty scenario; $\boldsymbol{x}$ is a vector of DA decision variables, mainly including on/off indicators $\alpha_t^{ng}$, $\alpha_t^{gt}$, $\alpha_t^{m}$, and $\alpha_t^{gs}$, startup indicators $u_t^{ng}$, $u_t^{gt}$, and $u_t^{m}$, and DA trading power $P_t^{Bda}$ and $P_t^{Sda}$; $\boldsymbol{y}_s$ is a vector of intraday decision variables, mainly including the outputs of LNG equipment and flexible resources, as well as the intraday HA electricity transactions; $\boldsymbol{u}_s$ is a vector of uncertainty variables including $P_t^{ren}$, $P_t^{ld}$, $N_t^{ld}$, and $CO_t^{ld}$.

In (44), the first "min" term is to minimize the DA cost, and the second "min" term is to minimize the average intraday HA operation cost with respect to multiple uncertainty scenarios. Furthermore, constraint (45) summarizes (3), (4), (30), (34), (35), and (41). Equation (46) groups (2), (9)-(11), (13), (15), (19)-(21), (25), (26), (29), (31)-(33), and (36)-(39). Finally, constraints (1), (5), (12), (16)-(18), (22)-(24), (27), (40), (42), and (43) form (47).

As previously noted, it is not always true to presume the reoccurrence of historical events, whereas it is reasonable to assume that the uncertainty realization is likely to occur around each scenario within a narrow variation interval. In the proposed DDSR solution method, each scenario is regarded as a reference profile, which is further used to construct an interval. The interval can facilitate the worst-case searching to trace the trajectory of the uncertainty profile. The solution will seek the worst case in each interval as well as the corresponding worst probability of occurrence with the overall variation control. Accordingly, a scenario uncertainty set for the worst-case scenario searching and a probability set for the worst-case distribution searching are designed.

### *A. Scenario Uncertainty Set*

The scenarios are used to create intervals whose lower and upper bounds are defined as the ratios of uncertainty profiles. Moreover, due to multiple uncertainty profiles, two different uncertainty budgets, i.e., the horizontal budget and the vertical budget, are established to constrain the variation level of the worst-case scenarios. The horizontal budget calculates the overall variation of each worst-case scenario across all scheduling periods of a day, while the vertical budget quantifies the average variation across all worst-case scenarios during each scheduling period. The scenario uncertainty set $\boldsymbol{U}$ is defined as:

$$\boldsymbol{U} = \left\{ \boldsymbol{u}_{t,s} \left| \begin{array}{ll} \underline{\boldsymbol{u}}_{t,s} \le \boldsymbol{u}_{t,s} \le \bar{\boldsymbol{u}}_{t,s} & \forall t, \forall s \\ \underline{\mu}_t \le \sum_{t=1}^{T} \dfrac{\boldsymbol{u}_{t,s}}{\hat{\boldsymbol{u}}_{t,s}} \le \bar{\mu}_t & \forall s \\ \underline{\varpi}_s \le \dfrac{1}{N_s} \sum_{s=1}^{N_s} \dfrac{\boldsymbol{u}_{t,s}}{\hat{\boldsymbol{u}}_{t,s}} \le \bar{\varpi}_s & \forall t \end{array} \right. \right\} \tag{48}$$

where $\hat{\boldsymbol{u}}_{t,s}$ is the vector of uncertainties under the expected values; $\underline{\boldsymbol{u}}_{t,s}$ and $\bar{\boldsymbol{u}}_{t,s}$ are the lower and upper bound vectors of the uncertainty interval, respectively; $\underline{\mu}_t$ and $\bar{\mu}_t$ are the lower and upper bounds of the horizontal budget, respectively; and $\underline{\varpi}_s$ and $\bar{\varpi}_s$ are the lower and upper bounds of the vertical budget, respectively.

In (48), the first constraint limits the range of uncertainty variables. The second and third constraints limit the horizontal and vertical budgets within the allowed ranges. For renewable energy generation and different loads, separate scenario uncertainty sets are constructed.

### *B. Probability Set*

Each worst-case scenario has the corresponding probability of occurrence, but in practice, the probability distribution may remain unknown. Thus, a probability set is constructed to characterize the ambiguous distribution, where the worst-case probability for each scenario is explored. According to [22], [23], $L_1$ and $L_\infty$ norms are used to measure the convergence rate of the distance between the true distribution and the empirical distribution, which can be approximately expressed as:

$$\begin{cases} Pr\left\{ \left\| \boldsymbol{\rho} - \boldsymbol{\rho}^0 \right\|_1 \le \theta_1 \right\} \ge 1 - 2N_s \mathrm{e}^{-2\theta_1} \\ Pr\left\{ \left\| \boldsymbol{\rho} - \boldsymbol{\rho}^0 \right\|_\infty \le \theta_\infty \right\} \ge 1 - 2N_s \mathrm{e}^{-2N_s\theta_\infty} \end{cases} \tag{49}$$

where $Pr\{\cdot\}$ is the probability distribution; $\boldsymbol{\rho}$ and $\boldsymbol{\rho}^0$ are the true distribution and the empirical distribution, which are the vectors composed of $\rho_s$ and $\rho_s^0$, respectively; and $\theta_1$ and $\theta_\infty$ are the tolerance parameters. Given the pre-set confidence levels $\beta_1$ and $\beta_\infty$, $\theta_1$ and $\theta_\infty$ can be calculated by setting the right-hand side of (49) to be the confidence levels as:

$$\begin{cases} \theta_1 = \dfrac{1}{2} \ln \dfrac{2N_s}{1-\beta_1} \\ \theta_\infty = \dfrac{1}{2N_s} \ln \dfrac{2N_s}{1-\beta_\infty} \end{cases} \tag{50}$$

Based on the above formulas, the probability set $\boldsymbol{D}$ is expressed as:

$$\boldsymbol{D} = \left\{ \rho_s \left| \begin{array}{ll} \sum_{s=1}^{N_s} \rho_s = 1 & \\ \rho_{\min} \le \rho_s \le 1 & \forall s \\ \left\| \boldsymbol{\rho} - \boldsymbol{\rho}^0 \right\|_1 \le \theta_1 & \\ \left\| \boldsymbol{\rho} - \boldsymbol{\rho}^0 \right\|_\infty \le \theta_\infty & \end{array} \right. \right\} \tag{51}$$

where $\rho_{\min}$ is the minimum probability for each identified scenario. To maintain statistical consistency and avoid subjective bias, a uniform distribution can be assigned to the empirical distribution $\boldsymbol{\rho}^0$ [24], [25]. In other words, the ini-

tial $\rho_s^0$ is equal to $1/N_s$. It is noteworthy that other probability distributions can be applied to $\boldsymbol{\rho}^0$ without compromising the effectiveness of the probability set.

### C. Data-driven Stochastic Robust Model with Benders Decomposition-based Solution Algorithm

The general form of the DDSR energy management model can be expressed as:

$$\begin{cases} \min\limits_{\boldsymbol{x}} \boldsymbol{A}^{\mathrm{T}}\boldsymbol{x} + \max\limits_{\rho_s \in \boldsymbol{D}, \boldsymbol{u}_s \in \boldsymbol{U}} \sum\limits_{s=1}^{N_s} \rho_s \min\limits_{\boldsymbol{y}_s} \boldsymbol{B}^{\mathrm{T}}\boldsymbol{y}_s \\ \text{s.t. (45)-(48), (51)} \end{cases} \tag{52}$$

The "max" term aims to seek the worst-case scenarios and the corresponding worst-case probabilities in the scenario uncertainty set and the probability set, respectively.

To solve (52), a Benders decomposition-based solution algorithm [27] is developed. It decomposes (52) into a master problem and a slave problem. The slave problem searches for the worst-case scenarios and the corresponding worst-case probabilities, while the master problem optimizes decision variables of MEMG energy management with the identified worst-case scenarios and probabilities. The overview of the proposed solution algorithm is illustrated in Fig. 2.

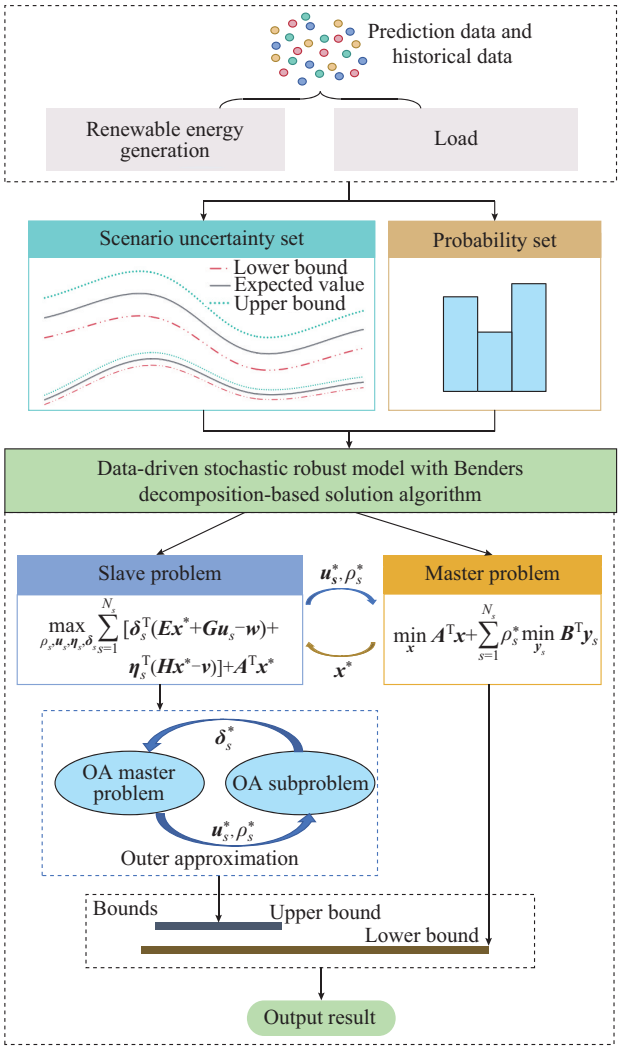


Fig. 2. Overview of proposed solution algorithm.

#### 1) Slave Problem

With the optimal DA decision variables $\boldsymbol{x}^*$, the slave problem is obtained by dualizing the inner "min" term in (52), given as:

$$\begin{cases} \max\limits_{\rho_s, \boldsymbol{u}_s, \boldsymbol{\eta}_s, \boldsymbol{\delta}_s} \sum\limits_{s=1}^{N_s} \left[ \boldsymbol{\delta}_s^{\mathrm{T}} \left( \boldsymbol{E}\boldsymbol{x}^* + \boldsymbol{G}\boldsymbol{u}_s - \boldsymbol{w} \right) + \boldsymbol{\eta}_s^{\mathrm{T}} \left( \boldsymbol{H}\boldsymbol{x}^* - \boldsymbol{v} \right) \right] + \boldsymbol{A}^{\mathrm{T}}\boldsymbol{x}^* \\ \text{s.t. (48), (51)} \\ \quad \rho_s \boldsymbol{B}^{\mathrm{T}} + \boldsymbol{\delta}_s^{\mathrm{T}} \boldsymbol{F} + \boldsymbol{\eta}_s^{\mathrm{T}} \boldsymbol{I} = 0 \quad \forall s \\ \quad \boldsymbol{\eta}_s \geq \boldsymbol{0} \quad \forall s \end{cases} \tag{53}$$

where $\boldsymbol{\delta}_s$ and $\boldsymbol{\eta}_s$ are the vectors of dual variables. The bilinear terms $\boldsymbol{\delta}_s^{\mathrm{T}}\boldsymbol{u}_s$ in the objective function (53) can be addressed by an outer approximation (OA) approach [28], which divides (53) into an OA master problem and an OA subproblem, given as follows.

Given the uncertainty $\boldsymbol{u}_s^*$ and the dual variable $\boldsymbol{\delta}_s^*$, the OA master problem is given as:

$$\begin{cases} \max\limits_{\rho_s, \boldsymbol{u}_s, \boldsymbol{\eta}_s, \boldsymbol{\delta}_s} \sum\limits_{s=1}^{N_s} \left[ \boldsymbol{\delta}_s^{\mathrm{T}} \left( \boldsymbol{E}\boldsymbol{x}^* - \boldsymbol{w} \right) + \boldsymbol{\eta}_s^{\mathrm{T}} \left( \boldsymbol{H}\boldsymbol{x}^* - \boldsymbol{v} \right) + \beta_s \right] + \boldsymbol{A}^{\mathrm{T}}\boldsymbol{x}^* \\ \text{s.t. (48), (51)} \\ \quad \rho_s \boldsymbol{B}^{\mathrm{T}} + \boldsymbol{\delta}_s^{\mathrm{T}} \boldsymbol{F} + \boldsymbol{\eta}_s^{\mathrm{T}} \boldsymbol{I} = 0 \quad \forall s \\ \quad \boldsymbol{\eta}_s \geq \boldsymbol{0} \quad \forall s \\ \quad \beta_s \leq \left( \boldsymbol{\delta}_s^* \right)^{\mathrm{T}} \boldsymbol{G}\boldsymbol{u}_s^* + \left( \boldsymbol{\delta}_s - \boldsymbol{\delta}_s^* \right)^{\mathrm{T}} \boldsymbol{G}\boldsymbol{u}_s^* + \left( \boldsymbol{u}_s - \boldsymbol{u}_s^* \right)^{\mathrm{T}} \boldsymbol{G}^{\mathrm{T}} \boldsymbol{\delta}_s^* \quad \forall s \end{cases} \tag{54}$$

By solving the OA master problem (54), the newly obtained $\boldsymbol{u}_s^*$ and $\rho_s^*$ are sent to the OA subproblem, and the OA upper bound $U^{OA}$ is updated.

Furthermore, the OA subproblem aims to update the dual variables, given as:

$$\begin{cases} \max\limits_{\boldsymbol{\eta}_s, \boldsymbol{\delta}_s} \sum\limits_{s=1}^{N_s} \left[ \boldsymbol{\delta}_s^{\mathrm{T}} \left( \boldsymbol{E}\boldsymbol{x}^* + \boldsymbol{G}\boldsymbol{u}_s^* - \boldsymbol{w} \right) + \boldsymbol{\eta}_s^{\mathrm{T}} \left( \boldsymbol{H}\boldsymbol{x}^* - \boldsymbol{v} \right) \right] + \boldsymbol{A}^{\mathrm{T}}\boldsymbol{x}^* \\ \text{s.t. (48), (51)} \\ \quad \rho_s^* \boldsymbol{B}^{\mathrm{T}} + \boldsymbol{\delta}_s^{\mathrm{T}} \boldsymbol{F} + \boldsymbol{\eta}_s^{\mathrm{T}} \boldsymbol{I} = 0 \quad \forall s \\ \quad \boldsymbol{\eta}_s \geq \boldsymbol{0} \quad \forall s \end{cases} \tag{55}$$

By solving this OA subproblem, the optimal results of $\boldsymbol{\eta}_s^*$ and $\boldsymbol{\delta}_s^*$ are obtained, and only $\boldsymbol{\delta}_s^*$ is sent to the OA master problem. Also, the OA lower bound $L^{OA}$ is updated.

These two linear problems are iteratively solved until the difference between $U^{OA}$ and $L^{OA}$ decreases to an accepted tolerance. The identified $\boldsymbol{u}_s^*$ and $\rho_s^*$ are sent to the master problem, and the upper bound is updated.

#### 2) Master Problem

Given the identified worst-case scenarios $\boldsymbol{u}_s^*$ and probabilities $\rho_s^*$, the master problem is formulated as:

$$\begin{cases} \min\limits_{\boldsymbol{x}} \boldsymbol{A}^{\mathrm{T}}\boldsymbol{x} + \sum\limits_{s=1}^{N_s} \rho_s^* \min\limits_{\boldsymbol{y}_s} \boldsymbol{B}^{\mathrm{T}}\boldsymbol{y}_s \\ \text{s.t. (45)-(47) with } \boldsymbol{u}_s^* \end{cases} \tag{56}$$

The objective of the master problem provides a lower bound, and the newly obtained $\boldsymbol{x}^*$ is passed to the slave problem.

Finally, the optimal results of the MEMG energy management can be achieved by iteratively solving the master problem and the slave problem until the gap between the upper and lower bounds converges to an accepted tolerance.

## VI. Case Study

### A. System Setting

The proposed DDSR energy management method is applied to an MEMG with the cascade utilization of LNG cold energy. The cascade utilization processes contain carbon capture, cryogenic power generation, and direct cooling. The parameters of the gasification station and the cascade utilization of LNG cold energy [19] are summarized in Table I. Moreover, the MEMG is equipped with renewable energy generators, gas storage tanks, electric chillers, and microturbines with parameters given in Table II.

TABLE I
Parameters of Gasification Station and Cascade Utilization of LNG Cold Energy

| Parameter | Value | Parameter | Value |
|---|---|---|---|
| $\rho_{ng}$ | 0.71 kg/m³ | $CE^{p}_{\min}$, $CE^{p}_{\max}$ | 200, 4000 kWh |
| $\eta_{ce}$ | 0.268 | $CE^{co}_{\min}$, $CE^{co}_{\max}$ | 30, 3000 kWh |
| $N^{ng}_{\min}$, $N^{ng}_{\max}$ | 10000, 120000 m³/h | $CE^{c}_{\min}$, $CE^{c}_{\max}$ | 50, 1000 kWh |
| $c_{ng}$ | 2.2 kJ/(kg·°C) | $\mu_c$, $\mu_p$, $\mu_{co}$ | 0.06, 0.1, 0.1 |
| $\Delta T$ | 180 °C | $k_c$, $k_p$, $k_{co}$ | 0.15, 0.18, 0.12 |
| $h$ | 530 kJ/kg | $\eta_c$, $\eta_p$, $\eta_{co}$ | 6, 0.6, 0.7 |
| $T^{ng}_{on}$, $T^{ng}_{off}$ | 3, 3 hours | $T^{m}_{on}$, $T^{m}_{off}$ | 3, 3 hours |
| $c^{lng}_{c}$ | 0.4 ¥/kg | $c^{lng}_{p}$ | 0.3 ¥/kW |
| $c^{lng}_{co}$ | 0.05 ¥/kWh | $c^{c}_{su}$, $c^{p}_{su}$, $c^{co}_{su}$, $c^{ng}_{su}$ | 50, 3, 20, 20 ¥/time |

TABLE II
Parameters of MEMG Equipment

| Equipment | Parameter | Value |
|---|---|---|
| Gas storage tank | $V_{gs}$ | 250 m³ |
| | $S^{gs}_{0}$, $S^{gs}_{24}$ | 0.5, 0.5 |
| | $S^{gs}_{\min}$, $S^{gs}_{\min}$ | 0.1, 0.9 |
| | $N^{gs}_{\max}$ | 30000 m³ |
| | $\eta_{gs}$ | 200 |
| | $k_{gs}$ | 0.05 |
| Electric chiller | $CO^{ec}_{\max}$ | 1800 kW |
| | $\eta_{ec}$ | 3 |
| Microturbine | $\eta^{gt}$ | 3 |
| | $c^{gt}_{su}$ | 105 ¥/time |
| | $P^{gt}_{\min}$, $P^{gt}_{\max}$ | 200, 1500 kW |
| | $r^{gt}_{\min}$, $r^{gt}_{\max}$ | 1000, 1000 kW |
| | $\lambda_{g.co2}$ | 2.16 kg/m³ |

The profiles of renewable energy generation (wind turbine) and loads (electric, cooling, and gas loads) are illustrated in Fig. 3. The maximum capacity of renewable energy generation is 1000 kW. The peak demands of electric, cooling, and gas loads are 4000 kW, 3000 kW, and 120,000 m³, respectively. The daily carbon emission limit is set to be 1000 kg. Based on these expected scenarios, the upper and lower bounds of renewable energy generation are set to be 1.2 and 0.8 of the expected values, respectively, while the upper and lower bounds of different loads are set to be 1.1 and 0.9 of the expected values, respectively. A total of 50 scenarios are randomly generated within these intervals to represent historical and prediction data. Then, the allowed variation range for each scenario is set between 1.05 and 0.95 of the scenario data. The upper and lower bounds of the horizontal or vertical budgets are set to be 1.03 and 0.97, respectively. $\rho_{\min}$ is set to be 0.01, and the confidence levels for both $\beta_1$ and $\beta_\infty$ are set to be 0.95.

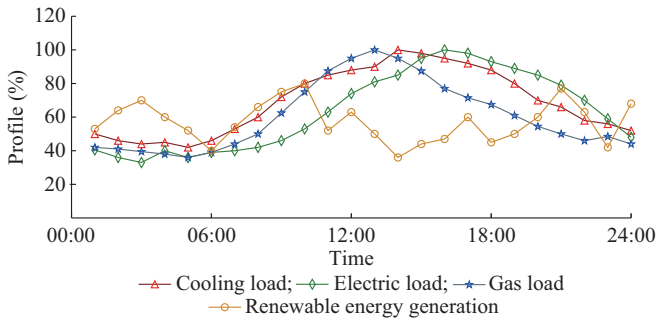


Fig. 3. Profiles of renewable energy generation and loads.

Moreover, the reference electricity prices are based on [29]. The DA purchasing and selling prices are set to be 1.1 and 0.9 of the reference prices, respectively, while the intraday purchasing and selling prices are set to be 1.3 and 0.7 of the reference electricity prices, respectively. The carbon tax price is set to be 0.5 ¥/kg [30]. The termination tolerance of the DDSR-based solution method is set to be 0.001.

The proposed MEMG energy management method is programmed using YALMIP [31] interface on the MATLAB platform and solved by the GUROBI solver [32]. The simulation is conducted on a 64-bit PC with a 2.5 GHz CPU and 16 GB RAM.

### B. Results of DA Scheduling

The data-driven stochastic robust model in (52) is solved by the DDSR-based solution method. After three iterations, the on/off states of LNG gasification, cascade utilization of LNG cold energy and microturbine, as well as the DA electricity transaction are determined. The total solution time is 4.27 s, which is fully compatible for practical use.

The DA electricity transaction results are shown in Fig. 4. The MEMG purchases electricity mainly during the periods of 00:00-01:00 and 10:00-23:00. A large quantity of purchasing transactions occur between 12:00 and 20:00, corresponding to the periods of large electricity demands of MEMG.

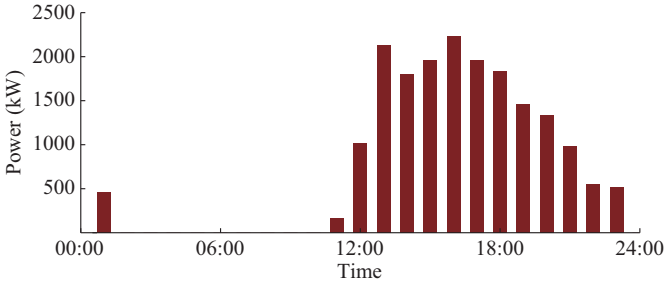


Fig. 4. DA electricity transaction results.

In response to the continuous NG demand, the LNG gasification facility is kept on throughout the day. The microturbine also remains in an active state for the entire day to

meet the electricity demand. Furthermore, the on/off states of the LNG cold energy utilization equipment are depicted in Fig. 5.

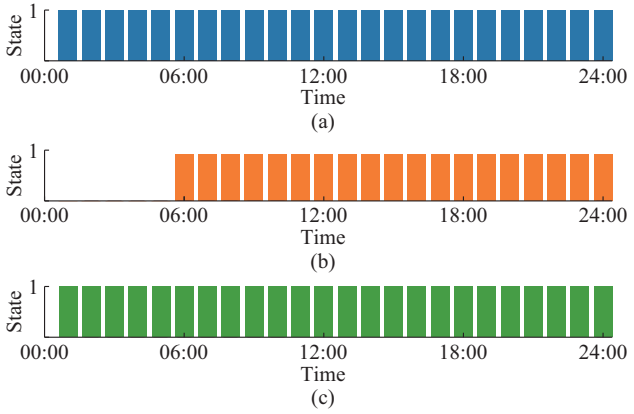


Fig. 5. On/off states of LNG cold energy utilization equipment. (a) Carbon capture stage. (b) Cryogenic power generation. (c) Direct cooling stage.

The first-stage carbon capture is fully activated as a result of efforts to reduce carbon emissions. The second-stage cryogenic power generation is suspended from 00:00 to 05:00 in the early morning when the electricity demand is relatively low. The third-stage direct cooling also remains activated throughout the entire day.

Additionally, the worst-case probabilities determined for 50 scenarios are illustrated in Fig. 6. It exhibits that scenarios 20, 22, 32, 40, 45, and 50 have high probabilities.

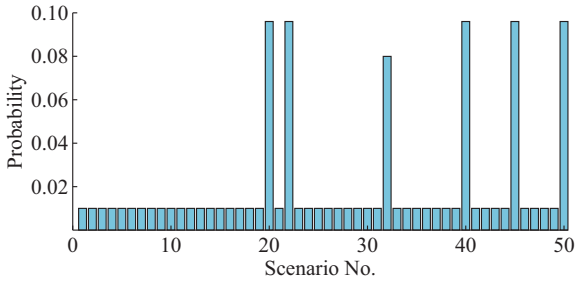


Fig. 6. Worst-case probabilities for 50 scenarios.

### C. Results of Intraday Operation

During the day, the outputs of all MEMG equipment and HA electricity transactions are optimized using more accurate predictions of renewable energy generation and loads, aiming to fulfill various load demands while simultaneously minimizing the overall operation costs and carbon emissions. Figure 7 shows the supply and demand of gas. The LNG gasification can primarily meet the gas demand with the assistance of gas storage tanks that enhance the flexibility in natural gas balancing and the required LNG cold energy. Moreover, Fig. 8 depicts the supply and demand of cooling. Given the high cooling demand during daytime hours, a substantial supply is derived from the direct cooling process of LNG cold energy. Additionally, as illustrated in Fig. 9, carbon emissions from microturbines can be fully captured during the day, realizing a zero-carbon emission.

Figure 10 shows the intraday electricity transactions in the HA electricity market. MEMG purchases electricity most of the time to eliminate the energy shortage while selling surplus electricity during the period of 00:00 to 01:00. Furthermore, the supply and demand of electricity are shown in Fig. 11. It indicates that cryogenic power generation, renewable energy generation and microturbine outputs all play significant roles in power supply. This helps reduce electricity purchases during high-price periods, thereby enhancing the economic benefits of the MEMG.

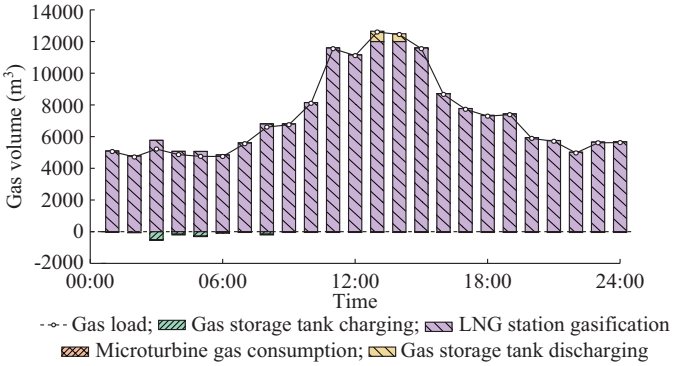


Fig. 7. Supply and demand of gas.

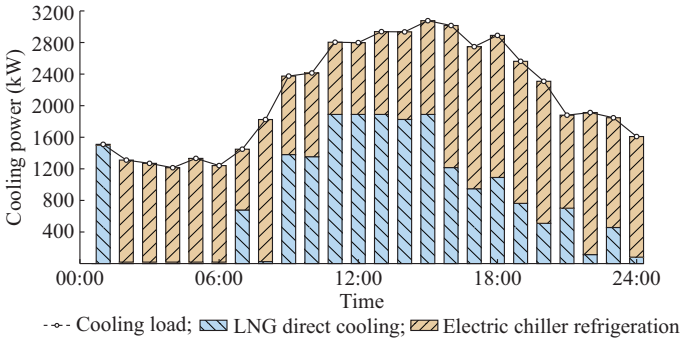


Fig. 8. Supply and demand of cooling.

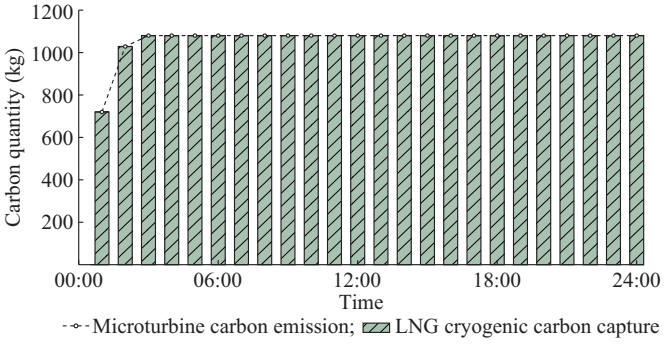


Fig. 9. Supply and demand of carbon.

### D. Sensitivity Analysis of Different Interval Widths with Feasibility Check

The uncertainty intervals of the scenario data play significant roles in the DDSR-based solution method. To evaluate the effect of different interval widths on the results, another two interval widths [0.98, 1.02] and [0.92, 1.08] of the scenario data are applied for comparison.

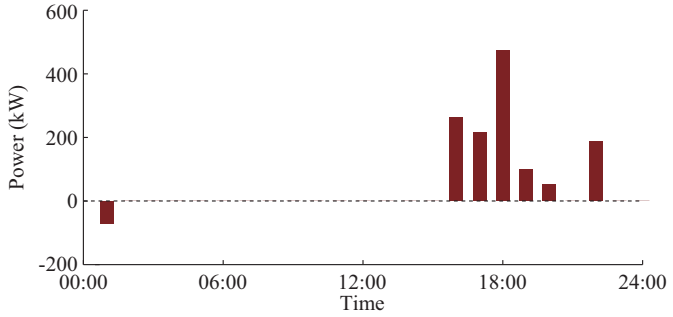


Fig. 10. Intraday electricity transactions in HA electricity market.

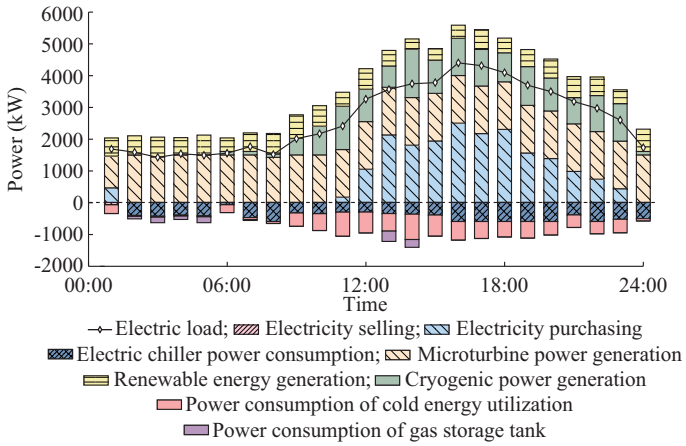


Fig. 11. Supply and demand of electricity.

To begin with, 500 scenarios of renewable energy generation power, electric load, cooling load, and gas load are randomly generated. Each scenario, regarded as an uncertainty realization, is consecutively fed into the intraday optimization process for a feasibility check. After solving all these scenarios, the average cost is calculated. Also, the infeasibility rate is determined by calculating the ratio of the unsuccessfully solved case number to the total scenario number.

The comparison results of different interval widths are shown in Table III.

TABLE III
COMPARISON RESULTS OF DIFFERENT INTERVAL WIDTHS

| Interval width | Average cost (¥) | Infeasibility rate (%) |
|---|---|---|
| [0.98, 1.02] | 26691.5 | 0 |
| [0.95, 1.05] | 26868.3 | 0 |
| [0.92, 1.08] | 27050.9 | 0 |

Table III shows that the proposed DDSR energy management method for the cascade utilization of LNG cold energy with different interval widths achieves zero infeasibility rate, showing high solution robustness. Moreover, it is evident that as the interval width expands, the average operation cost increases. This can be attributed to the fact that larger intervals tend to exacerbate the worst-case scenarios, resulting in more conservative solutions.

### *E. Comparison with Other Methods with Feasibility Check*

In this subsection, the previous 500 scenarios are continuously employed to demonstrate the advantages of the proposed DDSR energy management method for the multi-stage cascade utilization of LNG cold energy, compared with the single-stage utilization of LNG cold energy as well as various solution methods.

Firstly, the single-stage utilization (i.e., direct cooling) of LNG cold energy is applied for comparative analysis. The characteristics and parameters of other equipment in MEMG remain unchanged. The comparison results are given in Table IV. It is illustrated that the proposed DDSR energy management method for the multi-stage cascade utilization of LNG cold energy can achieve a low operation cost, indicating the improvement of energy utilization efficiency.

TABLE IV
COMPARISON RESULTS OF SINGLE-STAGE AND MULTI-STAGE CASCADE UTILIZATIONS OF LNG COLD ENERGY

| Cascade utilization of LNG cold energy | Average cost (¥) |
|---|---|
| Single-stage | 31020.2 |
| Multi-stage | 26868.3 |

Additionally, the DDSR-based solution method is compared with three other solution methods, which are described as follows.

Method 1: the SO method. The uncertainties are modelled using randomly generated scenarios.

Method 2: the RO method. A column-and-constraint generation [33] solution algorithm is applied to seek the worst case and solve the problem.

Method 3: the data-driven distributionally robust optimization (DRO) method [23] using 1- and ∞-norms for the ambiguity set.

Table V shows the comparison results of the average costs and infeasible rates of different solution methods.

TABLE V
COMPARISON RESULTS OF AVERAGE COSTS AND INFEASIBLE RATES OF DIFFERENT SOLUTION METHODS

| Method | Average cost (¥) | Infeasibility rate (%) |
|---|---|---|
| Method 1 | 26754.3 | 4 |
| Method 2 | 27874.3 | 0 |
| Method 3 | 27230.0 | 0 |
| DDSR-based solution method | 26868.3 | 0 |

As shown in Table V, Method 1 has the lowest operation cost, but there exists an infeasibility rate of 4%. This is because the SO method primarily focuses on the optimal expected solution rather than solution robustness. In contrast, the results of Method 2 exhibit high robustness against uncertainties, but the operation cost is also the highest, due to the consideration of the worst-case scenario in a large prediction interval. Furthermore, the average cost of Method 3 lies between those in Methods 1 and 2, while also achieving zero infeasible cases. This could be attributed to the fact that the data-driven DRO optimizes the decision across multiple uncertainty scenarios under the worst probability distribution.

In comparison, the DDSR-based solution method achieves

a relatively low operation cost, marginally higher than that of Method 1 and lower than that of Method 3, with full feasibility. This demonstrates superior performance in cost reduction and robustness for MEMG energy management.

To conclude, the proposed DDSR energy management method for the multi-stage cascade utilization of LNG cold energy can achieve economic advantages and solution robustness against uncertainties.

## VII. Conclusion

To efficiently harness the released cold energy during LNG gasification, this paper proposes a DDSR energy management method for the MEMG of an LNG receiving terminal. To model the cascade utilization of LNG cold energy, a general scheduling model considering the flexible coupling between adjacent stages, energy losses, and electric power consumption is proposed, which is further applied to the multi-stage cascade utilization of carbon capture, cryogenic power generation, and direct cooling. Moreover, a two-stage energy management framework is introduced to coordinate the cascade utilization of LNG cold energy with other energy resources in the MEMG, aiming to minimize operation costs and carbon emissions. Considering the uncertainties of renewable generation and various load demands, a DDSR-based solution method is developed to search for the worst-case scenarios and their corresponding worst-case probability based on the prediction data and the historical data. Accordingly, a Benders decomposition-based solution algorithm is developed to decompose the problem into a master problem and a slave problem, which are solved iteratively.

Through the simulation, the proposed DDSR energy management method outperforms the single-stage cascade utilization of LNG cold energy, showing great economic benefits with improved energy utilization efficiency. Furthermore, by implementing a feasibility check, compared with the conventional SO, RO, and DRO methods, the DDSR-based solution method in this paper exhibits superior performance in terms of cost reduction and solution robustness against uncertainties. In future work, the integration of alternative energy storage systems such as battery energy storage or thermal storage can be explored to further enhance the performance of MEMG operation.

## References


[1] Y. Cao, L. Qiang, Y. Tan *et al*., "A comprehensive review of energy internet: basic concept, operation and planning methods, and research prospects," *Journal of Modern Power Systems and Clean Energy*, vol. 6, no. 3, pp. 399-411, May 2018.

[2] T. He, Z. Chong, J. Zheng *et al*., "LNG cold energy utilization: prospects and challenges," *Energy*, vol. 170, pp. 557-568, Mar. 2019.

[3] T. He, N. Mao, M. Qi *et al*., "Exploring the stability and dynamic responses of dual-stage series orc using LNG cold energy for sustainable power generation," *Applied Energy*, vol. 372, p. 123735, Oct. 2024.

[4] F. Wang, P. Li, L. Gai *et al*., "Enhancing the efficiency of power generation through the utilisation of LNG cold energy by a dual-fluid condensation Rankine cycle system," *Energy*, vol. 305, p. 132113, Oct. 2024.

[5] X. Zheng, Y. Li, J. Zhang *et al*., "Design and multi-objective optimization of combined air separation and ORC system for harnessing LNG cold energy considering variable regasification rates," *International Journal of Hydrogen Energy*, vol. 57, pp. 210-223, Feb. 2024.

[6] X. Wang, L. Zhao, L. Zhang *et al*., "A novel combined system for LNG cold energy utilization to capture carbon dioxide in the flue gas from the magnesite processing industry," *Energy*, vol. 187, p. 115963, Nov. 2019.

[7] R. Zhang, C. Wu, W. Song *et al*., "Energy integration of LNG light hydrocarbon recovery and air separation: process design and techno-economic analysis," *Energy*, vol. 207, p. 118328, Sept. 2020.

[8] W. Lin, M. Huang, and A. Gu, "A seawater freeze desalination prototype system utilizing LNG cold energy," *International Journal of Hydrogen Energy*, vol. 42, no. 29, pp. 18691-18698, Jul. 2017.

[9] T. He, H. Lv, Z. Shao *et al*., "Cascade utilization of LNG cold energy by integrating cryogenic energy storage, organic Rankine cycle and direct cooling," *Applied Energy*, vol. 277, p. 115570, Nov. 2020.

[10] J. Pan, M. Li, R. Li *et al*., "Design and analysis of LNG cold energy cascade utilization system integrating light hydrocarbon separation, organic Rankine cycle and direct cooling," *Applied Thermal Engineering,* vol. 213, p. 118672, May 2022.

[11] X. Zheng, J. Zhang, Y. Li *et al*., "Performance analysis and multi-objective optimization for an integrated air separation, power generation, refrigeration and ice thermal storage system based on the LNG cold energy utilization," *International Journal of Refrigeration*, vol. 168, pp. 521-536, Jul. 2024.

[12] D. Li, G. Yin, W. Gao *et al*., "Role of $CO_2$-based mixtures in the organic Rankine cycle using LNG cold energy," *Sustainable Energy Technologies and Assessments*, vol. 65, p. 103752, May 2024.

[13] T. Wan, W. Zhou, B. Bai *et al*., "Evaluations of energy, exergy, and economic (3E) on a liquefied natural gas (LNG) cold energy utilization system," *International Journal of Hydrogen Energy*, vol. 65, pp. 308-318, May 2024.

[14] T. Zhao, S. F. Ahmad, M. K. Agrawal *et al*., "Design and thermo-enviro-economic analyses of a novel thermal design process for a CCHP-desalination application using LNG regasification integrated with a gas turbine power plant," *Energy*, vol. 295, p. 131003, May 2024.

[15] M. Qi, J. Park, J. Kim *et al*., "Advanced integration of LNG regasification power plant with liquid air energy storage: enhancements in flexibility, safety, and power generation," *Applied Energy*, vol. 269, p. 115049, Jul. 2020.

[16] X. Chen, "Green and low-carbon energy-use," *The Innovation Energy*, vol. 1, no. 1, p. 100003, Feb. 2024.

[17] S. Li, D. Cao, W. Hu *et al*., "Multi-energy management of interconnected multi-microgrid system using multi-agent deep reinforcement learning," *Journal of Modern Power Systems and Clean Energy*, vol. 11, no. 5, pp. 1606-1617, Sept. 2023.

[18] H. Khaloie and F. Vallée, "Day-ahead dispatch of liquid air energy storage coupled with LNG regasification in electricity and LNG markets," *IEEE Transactions on Power Systems*, vol. 39, no. 3, pp. 5177-5190, May 2024.

[19] H. Hou, Y. Xie, M. Kam *et al*., "Bi-layer uncertainty economic scheduling for port multi-energy microgrid with cold energy cascade utilization," *Automation of Electric Power Systems*, vol. 48, no. 6, pp. 205-215, Mar. 2025.

[20] B. Wang, C. Zhang, X. Chen *et al*., "Price-based demand response supported three-stage hierarchically coordinated voltage control for microgrids," *Journal of Modern Power Systems and Clean Energy*, vol. 13, no. 1, pp. 338-350, Jan. 2025.

[21] P. Li, Z. Wu, C. Zhang *et al*., "Multi-timescale affinely adjustable robust reactive power dispatch of distribution networks integrated with high penetration of PV," *Journal of Modern Power Systems and Clean Energy*, vol. 11, no. 1, pp. 324-334, Jan. 2023.

[22] C. Zhao and Y. Guan, "Data-driven stochastic unit commitment for integrating wind generation," *IEEE Transactions on Power Systems*, vol. 31, no. 4, pp. 2587-2596, Jul. 2016.

[23] F. Li, D. Wang, H. Guo *et al*., "Distributionally robust optimization for integrated energy system accounting for refinement utilization of hydrogen and ladder-type carbon trading mechanism," *Applied Energy*, vol. 367, p. 123391, Aug. 2024.

[24] P. M. Esfahani and D. Kuhn, "Data-driven distributionally robust optimization using the Wasserstein metric: performance guarantees and tractable reformulations," *Mathematical Programming*, vol. 171, pp. 115-166, Jul. 2017.

[25] M. Mahmoodi, S. M. N. R. Abadi, A. Attarha *et al*., "Data-driven distributionally adjustable robust chance-constrained DG capacity assessment," *Journal of Modern Power Systems and Clean Energy*, vol. 12, no. 1, pp. 115-127, Jan. 2024.

[26] C. Zhang, Y. Xu, and Z. Y. Dong, "Probability-weighted robust optimization for distributed generation planning in microgrids," *IEEE Transactions on Power Systems*, vol. 33, no. 6, pp. 7042-7051, Nov. 2018.

[27] D. Bertsimas, E. Litvinov, X. Sun *et al*., "Adaptive robust optimization for the security constrained unit commitment problem," *IEEE Transactions on Power Systems*, vol. 28, no. 1, pp. 52-63, Feb. 2013.
[28] B. Wang, C. Zhang, C. Li *et al*., "Transactive energy sharing in a microgrid via an enhanced distributed adaptive robust optimization approach," *IEEE Transactions on Smart Grid*, vol. 13, no. 3, pp. 2279-2293, May 2022.
[29] B. Wang, C. Zhang, C. Li *et al*., "Hybrid interval-robust adaptive battery energy storage system dispatch with SoC interval management for unbalanced microgrids," *IEEE Transactions on Sustainable Energy*, vol. 13, no. 1, pp. 44-55, Jan. 2022.
[30] Y. Li, M. K. Lim, J. Hu *et al*., "Investigating the effect of carbon tax and carbon quota policy to achieve low carbon logistics operations," *Resources, Conservation and Recycling*, vol. 154, p. 104535, Mar. 2020.
[31] J. Lofberg, "YALMIP: a toolbox for modeling and optimization in MATLAB," in *Proceedings of 2004 IEEE International Conference on Robotics and Automation*, Taipei, China, Sept. 2004, pp. 284-289.
[32] Gurobi. (2025, Aug.). Gurobi. [Online]. Available: https://www.gurobi.com
[33] B. Zeng and L. Zhao, "Solving two-stage robust optimization problems using a column-and-constraint generation method," *Operations Research Letters*, vol. 41, no. 5, pp. 457-461, Sept. 2013.

**Bo Wang** received the B. E. (hons.) degree in electrical engineering, the M.Eng.Sc. degree in energy systems, and the Ph.D. degree in electrical engineering from the University of New South Wales (UNSW), Sydney, Australia, in 2013, 2014, and 2022, respectively. He is currently a Lecturer with the School of Electrical and Power Engineering, Hohai University, Nanjing, China. His research interests include planning and operation of distribution network and microgrid, transactive energy, energy-use net, and application of optimization theory and machine learning.

**Zhehan Jia** is currently pursuing the M.Sc. degree in electrical engineering and automation at Hohai University, Nanjing, China. Her research interests include modeling and optimization of modern power system, particularly in integrated energy system and multi-energy microgrid.

**Xingying Chen** received the B.Eng. degree from Southeast University, Nanjing, China, the M.Eng. degree from Hohai University, Nanjing, China, and the Ph. D. degree from Southeast University, in 1984, 1995, and 2002, respectively, all in electrical engineering. She joined the faculty of Hohai University in 1984, and has become a Full Professor since 2002. Her current research interests include distribution and utilization system of electric power, electricity market, energy management and control, energy economics, and energy-use net.

**Lei Gan** received the B. S. and Ph. D. degrees from North China Electric Power University, Beijing, China, in 2010 and 2017, respectively, both in electrical engineering. Since 2017, he has been with the School of Electrical and Power Engineering, Hohai University, Nanjing, China, where he is currently an Associate Professor. His research interests include power system planning and operation, and integrated energy system operation.

**Haochen Hua** received the B. Sc. degree in mathematics with finance and the Ph.D. degree in mathematical sciences from the University of Liverpool, Liverpool, U. K., in 2011 and 2016, respectively. From 2016 to 2020, he was a Postdoctoral Fellow with the Research Institute of Information Technology, Tsinghua University, Beijing, China. Since 2020, he has been a Professor with the School of Electrical and Power Engineering, Hohai University, Nanjing, China. His research interests include energy-use net, energy management and control, energy economics, and stochastic optimal and robust control theory.

**Kun Yu** received the B. Eng. and M. Eng. degrees from Hohai University, China, in 2000 and 2003, respectively, and the Ph.D. degree from Zhejiang University, Hangzhou, China, in 2011, all in electrical engineering. He joined the faculty of Hohai University in 2003, and has become a Full Professor since 2023. His current interests include self-healing control and optimal dispatching of smart distribution networks, efficient operation of energy-use net and energy economics, and energy-use net.

**Jun Shen** received the Ph.D. degree from Hebei University of Technology, Tianjin, China, in 2009. She carried out research on refrigeration and cryogenic technology at the Institute of Physical and Chemical Technology, Chinese Academy of Sciences, Beijing, China. She is currently a Professor and Doctoral Supervisor at Beijing Institute of Technology, Beijing, China, where she has also served as the Director of the Institute of Refrigeration and Cryogenic Engineering since 2022. Her current research interests include emerging refrigeration technologies, with a particular emphasis on magnetic refrigeration.